RSC Advances

ROYAL SOCIETY OF CHEMISTRY

www.rsc.org/advances

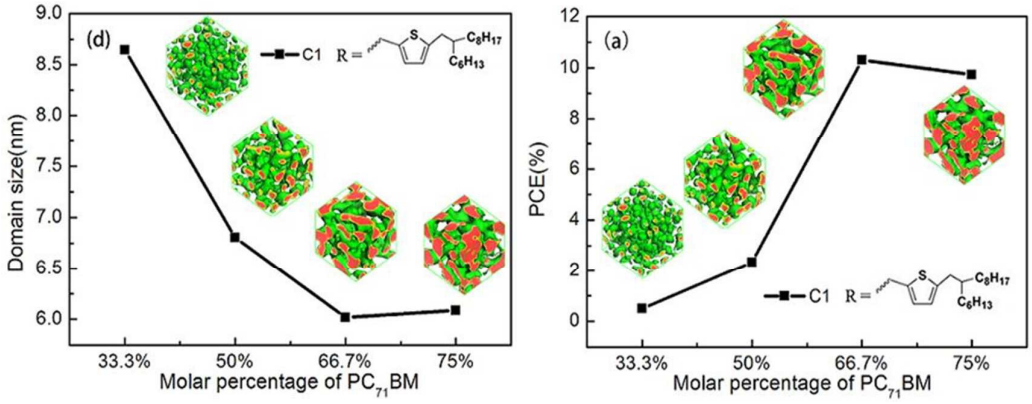

The predicted morphology, domain size, PCE (power conversion efficiency) of Small Molecular Organic Solar Cells.

The Prediction of the morphology and PCE of Small Molecular Organic Solar Cells

Xiaojuan Xu, Yujin Ji, Chunmiao Du, Tingjun Hou, Youyong Li*

Institute of Functional Nano & Soft Materials (FUNSOM), Soochow University, Suzhou 215123, China

Email: yyli@suda.edu.cn

Abstract. The efficiency of bulk heterojunction (BHJ) solar cell depends strongly on the morphology of the electron donors and electron acceptors in the active layer. Here we use Dissipative Particle Dynamics (DPD) simulation to predict the donor−acceptor morphology and graph theory to predict the efficiency of small molecular organic solar cell (SM OSC). We focus on a recently reported small molecular organic solar cell based on a new molecule donor, DTS(PTTh$_2$)$_2$ and three molecules DR3TBDTT, DR3TBDTT-HD, and DR3TBD2T with a benzo[1,2-b:4,5-b'] dithiophene (BDT) unit. With our theoretical approach, we are able to study the critical factors affecting the morphology and efficiency such as, the chemical structure of the conjugated molecular, fullerene functional group, solvents, additives, blend ratio, and processing conditions (e.g., annealing temperature). Our results are consistent with experimental conclusions and provide useful guidelines for improving the efficiency of small organic solar cell.

Keywords: Small organic solar cell (SMOSC); morphology of the active layer; power conversion efficiency (PCE); Dissipative Particle Dynamics (DPD); Graph theory

1 Introduction

In the circumstance of lack of energy, as a new generation of solar cell, organic solar cells (OSCs) are attracting more and more attention worldwide due to their potential to be cost effective and flexible solar energy conversion devices.[1-4] In the past few years, many research efforts have been focused on polymer solar cells and impressive results were achieved.[5-10] To date, power conversion efficiencies (PCE) over 10% have been obtained for both solution-processed single-junction polymer solar cells and the tandem devices.[2] Small molecule OSCs are of great interest to the research community owing to the distinct advantages of small-molecule semiconductors, such as well-defined structures, and batch-to-batch stability.[3] With consistent effort, the PCE of small-molecule OSCs had been improved from 0.03% to 10.08% in the past few years.[11-25] However, there is still much work needed to be done to overcome the hurdles of low PCE of small-molecule OSCs.

In order to find ways to overcome these limitations, computational approaches have been utilized for deciphering the roles of different variables that could improve the PCE and lifetime of an OPV cell.[26] A number of such studies have focused on some or all of the pertinent steps in solar energy conversion in an OPV device. These steps in chronological order are: (1) the absorption of light and excitons (i.e., electron–hole pair) generation; (2) the diffusion of the excitons to an interface; (3) the separation of the excitons into electrons and holes; (4) the transport of these electrons and holes to their corresponding electrode; and (5) the transfer of electrons and holes from the electrode to an external circuit. It is believed that the third step needs optimization in a bulk heterojunction (BHJ) design.[26] Here the design consists of a mixture of an electron donor and an electron acceptor (fullerene based molecules), which tends to form a phase segregated morphology. The phase segregation leads to a marked increase in the interfacial area between the donor and acceptor thus facilitating excitons separation. However, the ultimate goal is to achieve sizes of the

donor and electron acceptor domains commensurate with the excitons diffusion length so that a higher number of excitons can reach the donor–acceptor interface. The importance of the morphology of polymer bulk heterojunctions could be found in the reviews, such as, Liu *et al*.[27] and Ruderer and Mu¨ller-Buschbaum.[28]

Recently, three molecules named DR3TBDT-HD, DR3TBDTT and DR3TBD2T with a benzo[1,2-b:4,5-b'] dithiophene (BDT) unit and fullerene derivatives have been used as electron donor and acceptor materials.[29,30] The effects of blend ratio[31], additives[32,33] have been investigated to improve its morphology and efficiency. However, it is not clear how the chemical structures and the processing conditions affect the morphology and the efficiency. Here we combine DPD simulations and graph theory to predict the morphology and the efficiency of these small molecules organic solar cells. We study the effects of blend ratio of donor/$PC_{71}BM$, the annealing temperature of system, the additives, and the desolvation process. Our results are consistent with experimental conclusions and provide useful guidelines for improving the efficiency of small organic solar cell.

2 Simulation methods

2.1 DPD simulation

DPD was first proposed by Hoogerbrugge and Koelman[34,35] and later improved by Groot and Warren[36]. It is essentially a coarse-grained molecular dynamics (CGMD) method with a stochastic thermostat. In the DPD method, each bead represents a group of atoms and their movements are governed by:

$$\frac{dr_i}{dt} = \mathrm{v}_i, m_i \frac{dv_i}{dt} = F_i \qquad (1)$$

Where v_i, r_i and F_i represent the velocity, position vectors and total force acting on bead, respectively. Due to the significant reduction in the number of degrees of freedom, DPD can be used to simulate complex systems for much longer time. The forces acting on each bead can be divided into three components: conservative forces

(F_{ij}^{C}), dissipative forces (F_{ij}^{D}) and random forces (F_{ij}^{R}).

$$F_i = \sum_{j \neq i} (F_{ij}^{C} + F_{ij}^{D} + F_{ij}^{R}) \tag{2}$$

All the three forces act only within a cut-off radius r_c, which is taken as the unit of length in the simulation. The conservative force represents a soft repulsive interaction in linear form:

$$\boldsymbol{F}_{ij}^{C} = \begin{cases} a_{ij}(1 - r_{ij})\hat{\mathbf{r}}_{ij} & (r_{ij} < 1) \\ 0 & (r_{ij} \geq 1) \end{cases} \tag{3}$$

Where $\mathbf{r}_{ij}=\mathbf{r}_j-\mathbf{r}_i$, $r_{ij} = |\mathbf{r}_{ij}|$ and $\hat{\mathbf{r}}_{ij}=\mathbf{r}_{ij}/|\mathbf{r}_{ij}|$. The parameters a_{ij}, which represent the maximum repulsion between beads i and j, can be related to the Flory–Huggins parameter as follows:

$$a_{ij}(T) = \begin{cases} a_{ii} + 3.497 k_B T \chi_{ij}(T) & (\rho = 3) \\ a_{ii} + 1.451 k_B T \chi_{ij}(T) & (\rho = 5) \end{cases} \tag{4}$$

Where ρ represents the bead density of the system and a_{ii} is the repulsion parameter between the same beads. By matching the compressibility of water, a_{ii} and ρ are related through

$$a_{ii} = \frac{75 k_B T}{\rho} \tag{5}$$

The dissipative forces F_{ij}^{D} are the drag forces and the random forces F_{ij}^{R} represent the thermal noise of the system:

$$F_{ij}^{D} = \begin{cases} -\gamma w^{D}(r_{ij})(\mathbf{r}_{ij} \cdot \mathbf{v}_{ij})\mathbf{e}_{ij} & (r_{ij} < 1) \\ 0 & (r_{ij} \geq 1) \end{cases} \tag{6}$$

$$F_{ij}^{R} = \begin{cases} \sigma w^{R}(r_{ij}) \mathbf{r}_{ij} \xi_{ij} & (r_{ij} < 1) \\ 0 & (r_{ij} \geq 1) \end{cases} \tag{7}$$

Where γ is the friction parameter, σ is the noise amplitude parameter and $\mathbf{v}_{ij}=\mathbf{v}_i-\mathbf{v}_j$. The following equations should be satisfied to ensure the canonical ensemble equilibrium conditions and the fluctuation–dissipation relation:

$$\omega^{R}(r_{ij}) = \left[\omega^{D}(r_{ij})\right]^{1/2} \tag{8}$$

$$\sigma^2 = 2\gamma k_B T \tag{9}$$

We use γ = 4.5, k_BT = 1, and thus σ = 3 according to Eq. (9). F_i^S acts between consecutive beads within the same molecule, and has the following form:

$$F_i^S = \sum_j C\mathbf{r}_{ij} \quad (10)$$

Where C is the spring constant, and C is set to be 4 in this paper. [37]

2.2 Predict the efficiency by using graph theory based on the morphology of the active layer

To improve the efficiency of organic solar cells, it is essential to understand the role of morphology and tailor fabrication process to get desired morphologies. Wodo *et al*.[38] provide a comprehensive suite of physically meaningful morphology descriptors, which reflect the complex nature of the BHJ and the underlying device physics. They formulate and implement a graph-based framework to efficiently construct this comprehensive suite. This approach is motivated by the equivalence between a discretized 2D/3D morphology image. These morphology descriptors are further classified according to the physical processes of the photovoltaic process: excitons diffusion, excitons dissociation into free charge carriers, and charge transport. We obtain the 3D morphology from our DPD simulation firstly. Then we use the following three descriptors[38] to characterize the discrete morphology. The descriptors are f_{abs}, f_{diss}, f_{out}.

f_{abs} ----Fraction of donor materials. Light is absorbed by the electron donor to generate the excited hole-electron pairs (excitons) in the active layer. We should find the fraction of donor materials.

$$f_{abs} = \frac{Donor}{Donor + Acceptor} \quad (11)$$

If there is only donor and acceptor in the morphology, we could use f_{abs} respectively. However, our study involves solvent/additive in addition to donor and acceptor. It is necessary for us to modify descriptor f_{abs} to indicate the fraction of average donor/acceptor density.

$$f'_{abs} = \frac{\overline{\rho}_D}{\rho}\frac{\overline{\rho}_A}{\rho} f_{abs} \quad (12)$$

($\overline{\rho}_D$: the average density of donor; $\overline{\rho}_A$: the average of density of acceptor).

f_{diss} ---- Fraction of photoactive material within 10 nm distance (excitons diffusion length) to the interface.

$$f_{diss} = \frac{Donor(\mathrm{Vd} < 10\,\mathrm{nm})}{Donor} \quad (13)$$

By finding the fraction of donor material within this distance to the donor–acceptor interface, we identify the fraction of donor material that can theoretically contribute to this stage. Donor material distributed beyond this distance to the interface has a significantly lower chance of being useful.

f_{out} ----Fraction of materials with useful domains connected to the electrode.

$$f_{out} = \frac{I_{rb}}{I} \quad (14)$$

Only regions with a connection to the electrode constitute paths for charge to travel and consequently can contribute to current generation. If charges are created in islands or "cul-de-sacs" with no direct connection to appropriate electrode, they eventually recombine.

Wodo *et al.* further define a "performance indicator" as product of these three fractions.

$$f = f_{abs} f_{diss} f_{out} \quad (15)$$

They imply that f is a good marker for $\mathrm{J_{sc}}$. $\mathrm{J_{sc}}$ is a direct measurement of the device performance. In addition, the magnitude of short circuit current density is a quantity which is strongly affected by the morphology.[39,40]

The size of the interface and the domain size affect the charge collection efficiency. When the interface area is big, the domain size will be small. There is an optimum interface area of the morphology for the efficiency. Young Min Nam *et al.*'s

experimental results[41] show that, when the domain size is about 6 nm, the active layer shows the optimum PCE. Meanwhile, Peter K. Watkins *et al.*[42] use dynamical Monte Carlo model to evaluate the relationship between interface area and efficiency. Watkins et al. evaluated the "excitons dissociation efficiency" and "charge collection efficiency" separately and they conclude that there is an optimum interface area. We use the relationship of interface area and internal quantum efficiency derived from Watkins *et al*. and the optimum domain size 6 nm based on Young Min Nam *et al*.'s experimental results. And the descriptor is defined as the following:

$$f_{\mathrm{int}erface} = \begin{cases} \dfrac{6000}{A} & A > 6000nm^2 \\ 1 & A \le 6000nm^2 \end{cases} \tag{16}$$

A is the interface area.

When we use graph theory to estimate the efficiency, we use the empirical factors ($f_{abs}, f_{diss}, f_{out}, f_{interface}$) to represent different factors affecting the efficiency. We don't explicitly consider the process of the generation of the excition, the dissociation of the excition, and the charge transfer. Thus our model doesn't include all the factors affecting the final efficiency and overestimates the final efficiency. For example, Lin *et al*. explicitly investigate the charge-transfer processes at pentacene-C60 interface by using simulations.[43] They found that the positional relationship between donor and acceptor materials plays a critical role for the charge-transfer process. It will be interesting and challenging to simulate the charge transfer process of small molecule OPV explicitly and incorporate the factor into our model to improve the accuracy of the estimated efficiency.

In summary, the power conversion efficiencies based on morphology descriptors is defined as:

$$PCE = f'_{abs} f_{diss} f_{out} f_{\mathrm{int}erface} \tag{17}$$

3 Models and Parameters

We model donor and acceptor molecules in a coarse-grained manner to simulate

these systems on a length scale that is large enough to examine the blend morphology, while retaining necessary details at molecular level. As shown in Figure 1, we model a donor using four coarse-grained beads. The acceptor or the solvent is represented by one bead. The additive (PDMS) is represented by three beads.

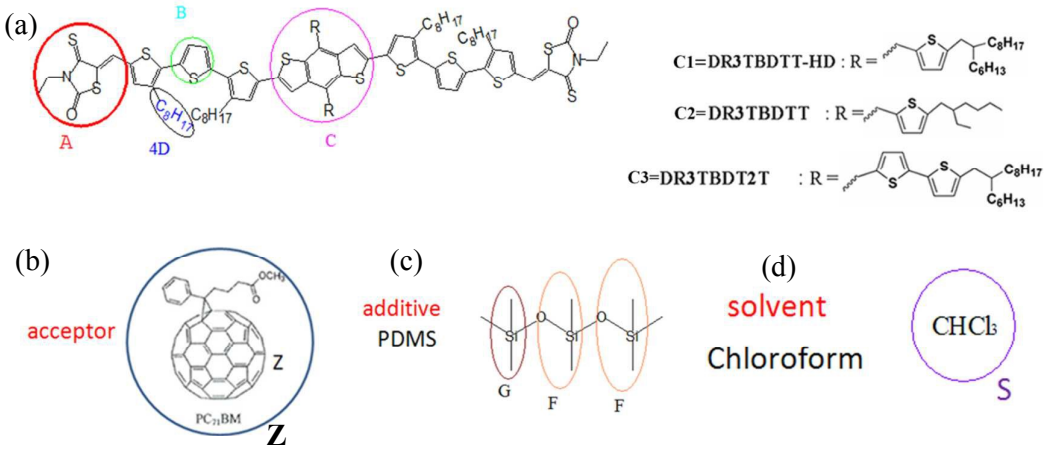

Figure 1. Chemical structures of donor, acceptor, solvent and additive are represented by coarse-grained beads. (a) Chemical structures of C1 (DR3TBDTT-HD), C2 (DR3TBDTT), C3 (DR3TBDT2T) [29] are represented by coarse-grained beads A, B, D, and C. (b) the fullerene derivative is represented by one coarse-grained bead Z. (c) The additive PDMS is represented by three coarse-grained beads, G, F, F. (d) the solvent chloroform is represented by one coarse-grained bead S.

Table 1. Parameters derived for the coase-grained beads defined in Figure 1.

	A	B	C1	C2	C3	D	S	F	G	Z
Solubility parameter	17.6	14.8	15.8	15.1	16.1	9.26	15.5	11.3	10.02	20.5
V_{mol}(Å)	170	82	923.5	579	1048.6	83.68	96.74	141.01	126.4	1003
M(g/mol)	130	84	872	578	956	29	29	89	58	1030

To obtain the solubility parameters and interaction potential parameters of

particles, we construct the amorphous structures of each fragment and perform molecular dynamics with COMPASS force-field [44,45] by using the Forcite module of Materials Studio software package to obtain cohesive energy, solubility parameters (δ_i)[46-48] and volume. According to Groot and Warren[49], we choose a standard volume of bead V_m, and this DPD bead is equal to N_m (real-space renormalization factor) water molecules (30Å^3). Then we obtain the length scale, time scale and the number of step. The formulas are listed as following:

$$r_c = \left(\rho \cdot V_{bead}\right)^{1/3} = \left(3\times 100\right)^{1/3} = 6.7\text{Å} = 0.67\text{nm} \quad (18)$$

$$\tau = \left(14.1 \pm 0.1\right) N_m^{\frac{5}{3}} = 103.55 ps \quad (19)$$

$$1000 \times N_m^{\frac{8}{3}} = 24000 \quad (20)$$

Table 2. the parameters of DPD simulation

Parameter	Value	Meaning
a_{ii}	25	Repulsion between identical particle types
T*	1.0	Reduced Temperature
V_m	100 Å^3	The volume of standard bead
N_m	3	Number of water molecules represented by one bead
δt	0.02	Time step
τ	103.55 ps	Characteristic time scale
r_c	0.67nm	Range of soft repulsive interaction
N	25000step	The number of step
C_S	4.0	Spring constant

The Newtonian equation of position and velocity of particles is solved by a modified version of the velocity Verlet algorithm.[50] In the simulation, the radius of interaction, the particle mass, and the temperature were chosen as $r_c = m = kT = 1$ and $\sigma = 3.67$, while the particle density $\rho = 3$ (taking into account the

computational efficiency, $\rho = 3$ is a reasonable choice).[34,35] The only parameter to be determined is the maximum repulsive force a_{ij}, which is chosen according to the linear relation with Flory-Huggins χ parameters.[51]

$$a_{ij} = a_{ii} + 3.27\chi \qquad a_{ii} = 25 \tag{21}$$

The Flory-Huggins χ parameter can be obtained from experiments, free energy of mixing, or solubility parameter[52,53]. Here we obtain the χ through the solubility parameter. And we obtain the solubility parameters from molecular dynamics (MD) simulations. A high-quality force field COMPASS (condensed-phase optimized molecular potentials for atomistic simulation studies)[54-56] is adopted, which is known to accurately reproduce experimental structures, densities, and solubility parameters.[57] MD simulations are performed under NPT thermodynamic ensemble. In our MD simulations, we obtain the cohesive energy (δ)[58]. Then we get the Flory-Huggins χ parameter by the equation (22).

$$\chi_{\mathrm{ij}} = \frac{V}{RT}\left(\delta_i - \delta_j\right)^2 \tag{22}$$

Where V is the arithmetic average of molar volumes of two beads, δ_i and δ_j are the solubility parameters of beads i and j, respectively. R is perfect gas constant. T is the temperature of system. Then we obtain the repulsive force a_{ij} according to the equation (21). The calculation results are listed in Table 3.

Table 3. the interaction parameters a_{ij} between beads at 346.4 K

	A	B	C	D	F	G	S	Z
A	25.00							
B	26.01	25.00						
C	26.86	25.52	25.00					
D	34.48	37.68	47.56	25.00				
F	31.87	25.57	25.14	25.43	25.00			
G	33.83	27.55	43.64	25.10	25.16	25.00		
S	25.62	25.05	25.05	28.70	27.40	28.50	25.00	
Z	28.92	37.75	43.64	58.35	45.83	27.40	35.10	25.00

In DPD method, the simulation length scale and time scale of molecular motions are much larger than ordinary molecular dynamics (MD) simulations. We choose the particle mass and the temperature and interaction range as units of mass, energy, and length, hence $r_c = m = kT = 1$, and the simulated time is expressed in the natural unit of time.[49] The simulation boxes of sizes in our DPD simulation is $32\times32\times 32 r_c^3$.

4. Result and discussion

4.1 The effect of the blend ratio on the morphology and the efficiency

The blend ratio of donor and acceptor is one of the most important factors affecting the morphology of BHJ solar cells. Jiaoyan Zhou *et al.*[29] , Yanming Sun[59] and Aung Ko Ko Kyaw[60] illustrated the importance of the ratio of small molecular donor/$PC_{71}BM$. Here we study the morphology and domain size of small molecular donor/ $PC_{71}BM$ for different composition ratio. Figure 2 shows the equilibrated morphology for different molar percentage of $PC_{71}BM$: 33.3%, 50%, 66.7%, and 75%. In addition, we studied three different small molecules C1, C2, C3 as the donor, as shown in Figure 2a, 2b, 2c respectively. The predicted efficiencies are summarized in Figure 2a, 2b, and 2c. The domain sizes are summarized in Figure 2d, 2e, and 2f.

Figure 2a, 2b, and 2c show consistent results that, when percentage of $PC_{71}BM$ is 66.7%, the efficiency is the highest. By analyzing the domain sizes as shown in Figure 2d, 2e, and 2f, we can see that when the domain size is around 6nm, the efficiency is good. In order to rationalize the different factors affecting the efficiency, we list the factors in Table 4.

As shown in Table 4, among the various factors, f_{out} is the most important factor for different blend ratios. When the percentage of $PC_{71}BM$ is 33.3% or 50%, the islands or 'cul-de-sacs' morphology is formed. Such morphology is poor for the fraction of useful domains connected to the electrode and leads to poor efficiency. Thus for 33.3% and 50%, f_{out} is low and the final efficiency is low. Meanwhile, when

the percentage of $PC_{71}BM$ is high, such as 75%, f_{abs} is limited, since the donor is responsible for absorbing the light. In conclusion, 66.7% percentage shows the best efficiency.

When Zhou *et al*.[29] made the device of C1, C2, C3 with $PC_{71}BM$, they chose the blend ratio as (1:0.8 w/w). It corresponds to the volume percentage of $PC_{71}BM$: 66.7%, which is the best blend ratio based on our results. Aung Ko Ko Kyaw *et al*. [60] studied the dependence on the percentage of PCBM. They concluded that, when the weight: weight ratio between $DTS(PTTh_2)_2$ and PCBM is 70:30 or 60:40 shows the best mobility and performance, which is close to our best blend ratio for C1, C2, C3 with $PC_{71}BM$: (1:0.8 w/w).

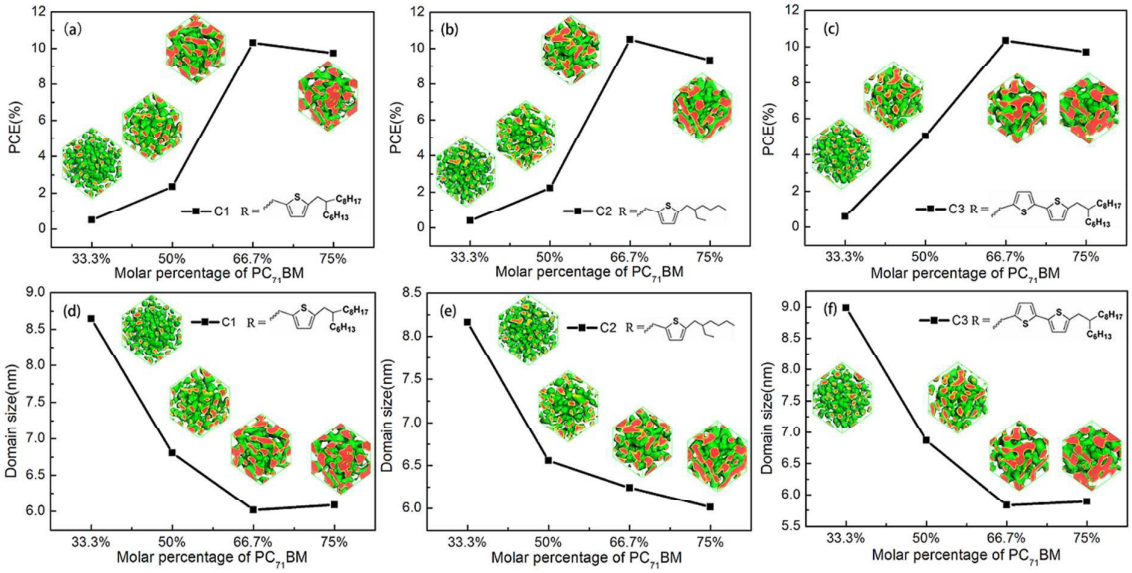

Figure 2. (a) The dependence of Power Conversion Efficiency (PCE) on the molar percentage of $PC_{71}BM$ for C1/$PC_{71}BM$; (b) The dependence of Power Conversion Efficiency (PCE) on the molar percentage of $PC_{71}BM$ for C2/$PC_{71}BM$; (c) The dependence of Power Conversion Efficiency (PCE) on the molar percentage of $PC_{71}BM$ for C3/$PC_{71}BM$; (d) The dependence of the domain size on the molar percentage of $PC_{71}BM$ for C1/$PC_{71}BM$; (e) The dependence of the domain size on the molar percentage of $PC_{71}BM$ for C2/$PC_{71}BM$; (f) The dependence of the domain size

on the molar percentage of $PC_{71}BM$ for C3/$PC_{71}BM$; Domain size is derived from the volume divided by the interface area. The optimum domain size favorable for efficiency is around 6nm.

Table 4 Morphology descriptors depends on the blend ratio of C1/$PC_{71}BM$

Factor	Molar percentage of $PC_{71}BM$	33.3%	50%	66.7%	75%
f_{abs}	Fraction of light absorbing material	89.6%	79.5%	64.8%	54.8%
f_{diss}	Fraction of photoactive material within d<10nm to the interface	81.8%	83.0%	87.5%	87.4%
f_{out}	Fraction of useful domains connected to the electrode	6.8%	22.9%	95.1%	97.8%
f	$f = f_{abs} * f_{diss} * f_{out}$	5.0%	15.1%	54.0%	46.8%
PCE	Power conversion efficiency	0.5%	2.3%	10.3%	9.7%

4.2 The effect of the annealing temperature on the morphology and the efficiency

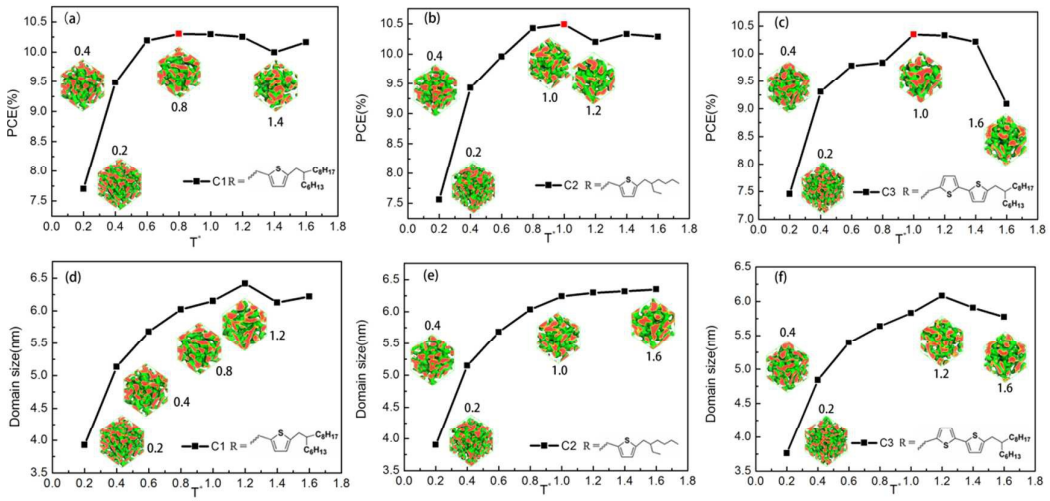

Figure 3. (a) The dependence of Power Conversion Efficiency (PCE) on the temperature of $PC_{71}BM$ for C1/$PC_{71}BM$; (b) The dependence of Power Conversion Efficiency (PCE) on the temperature for C2/$PC_{71}BM$; (c) The dependence of Power

Conversion Efficiency (PCE) on the temperature for C3/$PC_{71}BM$; (d) The dependence of the domain size on the temperature for C1/$PC_{71}BM$; (e) The dependence of the domain size on the temperature for C2/$PC_{71}BM$; (f) The dependence of the domain size on the temperature for C3/$PC_{71}BM$; The molar pencentage of $PC_{71}BM$ is 66.7%.

We then investigated how the annealing temperature affects the morphology, PCE and the domain size of SM OSC (see figure 3). In the DPD simulation, we set the reduced temperatures (T*) to the corresponding physical temperature. A rough but simple estimation of the value of this reduced temperature in terms of physical temperature can be given by the equation[61,62]: $T = 133T^* - 33$ to simplify the relationship between T and T*. The reduced temperatures T^*=0.2, 0.4, 0.6, 0.8, 1.0, 1.2, 1.4, and 1.6 correspond to physical temperature T=-6.4, 20.2, 46.8, 73.4, 100, 126.6, 153.2, and 179.8℃.

Figure 3 shows that the morphology and PCE are the best when the reduced temperatures is 1.0, namely, the physical temperature is 100 ℃ [63]. Similarly, temperature has been found to be an important parameter for morphology and efficiency, experimentally.[64,65] Upon changing the heating temperature, the extent of phase separation evolves and finally forms phase-separated network-like morphology, which benefits the efficiency of the device.

4.3 The effect of the additives on the morphology and the efficiency

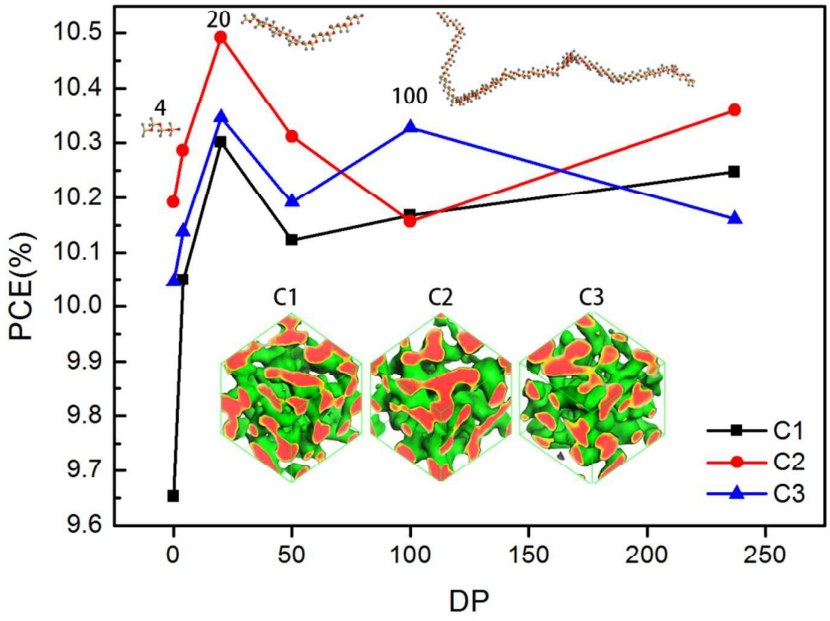

Figure 4. The dependence of the power conversion efficiency (PCE) on the degree of polymerization (DP) of PDMS as additive in the active layer formed by C1, C2, or C3 with $PC_{71}BM$. We highlight DP = 4, 20, or 100. When DP =20, it leads to the best PCE.

Kenneth R. Graham *et al.*[63] investigated the effect of macromolecular additive, polydimethylsiloxane (PDMS) on the performance of solution processed molecular bulk heterojunction solar cells. Their results show that PDMS has a strong influence on film morphology, with a significant decrease in film roughness and feature size observed. As a general, the additive has a higher solubility for $PC_{71}BM$ than the donor material.[32] This increases donor aggregation and leads to the formation of high ordered D and A phases, thus improving device performance.

Here we investigated how the Degree of Polymerization (DP) of PDMS affects the morphology and PCE of OSC. As shown in Figure 4, the introduction of PDMS will improve the PCE. For C1, C2, and C3, PCE will increase, when there is PDMS introduced. In addition, our results show that, when DP of PDMS is equal to 20, PCE

will be slightly better than other DP values (e.g. DP=4, or 100). This is consistent with Kenneth R. Graham's[66] results. Graham *et al*. showed that the PCE is enhanced from 1.42% without additive to 2.35% with 410 g/mol PDMS, which corresponds to DP around 4.4.

As summarized in Table 5, we can see that the domain size will increase as PCE, when there is PDMS introduced.[29] Our results show that, when there is PDMS introduced, *f* will increases, which corresponds to the short current. Our *f* values are consistent with the short current from experiments.[29] Our approach is useful to illustrate the effect of additives and will be useful for rational design of additives.

Table 5. The effect of the additive on the PCE, domain size, short current, and morphology descriptors

Donor:$PC_{71}BM$		**C1**		**C2**		**C3**	
		Without additive	**With additive**	**Without additive**	**With additive**	**Without additive**	**With additive**
PCE (%)	**Exptl.** [29]	6.07	6.50	7.22	7.80	11.66	11.73
	Modeling	6.95	10.30	10.19	10.49	10.04	10.35
Domain size (nm)	**Exptl.** [29]	15-35	20-45	10-30	15-40	8-30	15-35
	Modeling	5.76	6.02	6.26	6.24	5.79	5.83
J ($mA{\cdot}cm^{-2}$)	**Exptl.** [29]	12.16	11.75	12.92	12.95	11.66	11.73
***f* (%)**	**Modeling**	52.8	53.9	50.2	51.8	55.0	56.4

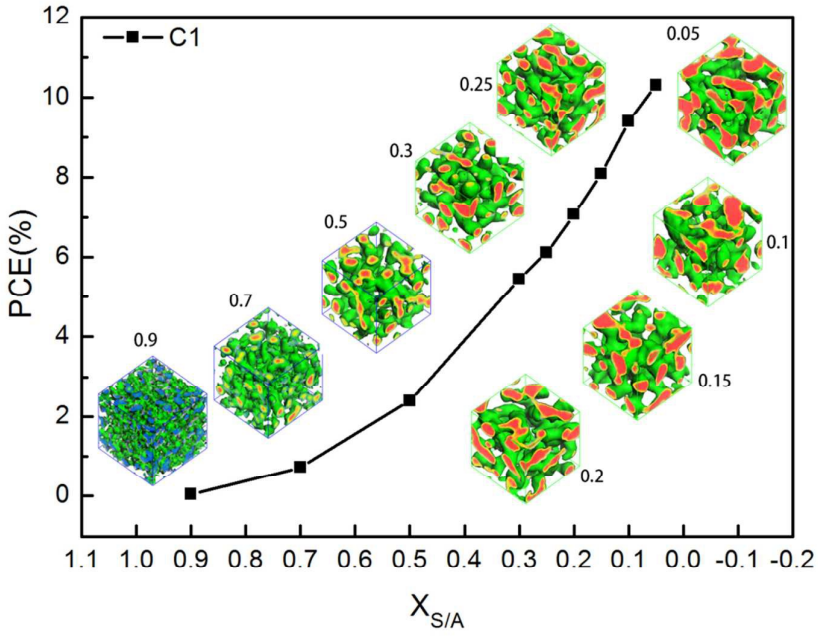

Figure 5. PCE and morphology of C1/$PC_{71}BM$ evaluated from DPD simulation and graph theory during desolvation process. $X_{S/A}$ represents the percentage of the solvent.

In addition, we studied the desolvation process based on DPD simulation and graph theory. Figure 5 shows the change of PCE and morphology during desolvation process. Based on our results, we can see that the aggregation level of $PC_{71}BM$ phase is becoming large with the evaporation of the solvent and percolating network of electron-donor and electron-acceptor materials is formed. And the PCE increases in the desolvation process. Our approach is able to provide the dynamical process during desolvation and will be useful for optimizing the desolvation procedure in the fabrication.

5 Conclusions

In this work, we use Dissipative Particle Dynamics simulation and Graph theory to predict the morphology and efficiency of small molecular organic solar cell. Our

simulations explore the effects of the structural parameters on the morphology. We compare our results with recent experiments and provide a quantitative and qualitative analysis for the experiments studies.

Certainly the Small molecule as the donor is the good choice for organic solar cells. In summary, we combine atomistic simulation with mesoscale simulation to predict the morphology of BHJ solar cells and the optimal parameters for morphology of BHJ solar cells. For the effect of the blend ratio, we find that the molar ratio of $PC_{71}BM$ 66.7% leads to the best performance. In addition, we study the effect of temperature and the additives on the morphology and the performance of small molecular organic solar cell. Our approach is useful to illustrate the mechanism and the important factors for organic solar cell. And it could be used to optimize other important factors to improve the performance of organic solar cell.

Acknowledgement

The work is supported by the National Basic Research Program of China (973 Program, Grant No. 2012CB932400), the National Natural Science Foundation of China (Grant No. 91233115, 21273158, and 91227201), a Project Funded by the Priority Academic Program Development of Jiangsu Higher Education Institutions (PAPD). This is also a project supported by the Fund for Innovative Research Teams of Jiangsu Higher Education Institutions, Jiangsu Key Laboratory for Carbon-Based Functional Materials and Devices, Collaborative Innovation Center of Suzhou Nano Science and Technology.

References

(1) Cheng, Y.-J.; Yang, S.-H.; Hsu, C.-S. Synthesis of conjugated polymers for organic solar cell applications. *Chemical Reviews* **2009**, *109*, 5868-5923.

(2) Li, G.; Zhu, R.; Yang, Y. Polymer solar cells. *Nature Photonics* **2012**, *6*, 153-161.

(3) Mishra, A.; Bäuerle, P. Small molecule organic semiconductors on the move: promises for future solar energy technology. *Angewandte Chemie International Edition* **2012**, *51*, 2020-2067.

(4) Po, R.; Maggini, M.; Camaioni, N. Polymer solar cells: recent approaches and achievements.

The Journal of Physical Chemistry C **2009**, *114*, 695-706.

(5) Bronstein, H.; Collado‐Fregoso, E.; Hadipour, A.; Soon, Y. W.; Huang, Z.; Dimitrov, S. D.; Ashraf, R. S.; Rand, B. P.; Watkins, S. E.; Tuladhar, P. S. Thieno [3, 2‐b] thiophene‐diketopyrrolopyrrole Containing Polymers for Inverted Solar Cells Devices with High Short Circuit Currents. *Advanced Functional Materials* **2013**, *23*, 5647-5654.

(6) Intemann, J. J.; Yao, K.; Li, Y. X.; Yip, H. L.; Xu, Y. X.; Liang, P. W.; Chueh, C. C.; Ding, F. Z.; Yang, X.; Li, X. Highly Efficient Inverted Organic Solar Cells Through Material and Interfacial Engineering of Indacenodithieno [3, 2‐b] thiophene‐Based Polymers and Devices. *Advanced Functional Materials* **2014**, *24*, 1465-1473.

(7) Li, W.; Hendriks, K. H.; Furlan, A.; Roelofs, W.; Meskers, S. C.; Wienk, M. M.; Janssen, R. A. Effect of the Fibrillar Microstructure on the Efficiency of High Molecular Weight Diketopyrrolopyrrole‐Based Polymer Solar Cells. *Advanced Materials* **2014**, *26*, 1565-1570.

(8) Cabanetos, C. m.; El Labban, A.; Bartelt, J. A.; Douglas, J. D.; Mateker, W. R.; Fréchet, J. M.; McGehee, M. D.; Beaujuge, P. M. Linear side chains in benzo [1, 2-b: 4, 5-b′] dithiophene–thieno [3, 4-c] pyrrole-4, 6-dione polymers direct self-assembly and solar cell performance. *Journal of the American Chemical Society* **2013**, *135*, 4656-4659.

(9) Li, K.; Li, Z.; Feng, K.; Xu, X.; Wang, L.; Peng, Q. Development of large band-gap conjugated copolymers for efficient regular single and tandem organic solar cells. *Journal of the American Chemical Society* **2013**, *135*, 13549-13557.

(10) Meager, I.; Ashraf, R. S.; Mollinger, S.; Schroeder, B. C.; Bronstein, H.; Beatrup, D.; Vezie, M. S.; Kirchartz, T.; Salleo, A.; Nelson, J. Photocurrent Enhancement from diketopyrrolopyrrole polymer solar cells through alkyl-chain branching point manipulation. *Journal of the American Chemical Society* **2013**, *135*, 11537-11540.

(11) Cha, H.; Chung, D. S.; Bae, S. Y.; Lee, M. J.; An, T. K.; Hwang, J.; Kim, K. H.; Kim, Y. H.; Choi, D. H.; Park, C. E. Complementary Absorbing Star‐Shaped Small Molecules for the Preparation of Ternary Cascade Energy Structures in Organic Photovoltaic Cells. *Advanced Functional Materials* **2013**, *23*, 1556-1565.

(12) Chen, Y.-H.; Lin, L.-Y.; Lu, C.-W.; Lin, F.; Huang, Z.-Y.; Lin, H.-W.; Wang, P.-H.; Liu, Y.-H.; Wong, K.-T.; Wen, J. Vacuum-deposited small-molecule organic solar cells with high power conversion efficiencies by judicious molecular design and device optimization. *Journal of the American Chemical Society* **2012**, *134*, 13616-13623.

(13) Leliège, A.; Grolleau, J.; Allain, M.; Blanchard, P.; Demeter, D.; Rousseau, T.; Roncali, J. Small D‐π‐A Systems with o‐Phenylene‐Bridged Accepting Units as Active Materials for Organic Photovoltaics. *Chemistry-A European Journal* **2013**, *19*, 9948-9960.

(14) Li, P.; Tong, H.; Ding, J.; Xie, Z.; Wang, L. Small molecules based on 2, 7-carbazole for efficient solution-processed organic solar cells. *Journal of Materials Chemistry A* **2013**, *1*, 8805-8812.

(15) Liu, J.; Sun, Y.; Moonsin, P.; Kuik, M.; Proctor, C. M.; Lin, J.; Hsu, B. B.; Promarak, V.; Heeger, A. J.; Nguyen, T. Q. Tri‐Diketopyrrolopyrrole Molecular Donor Materials for High‐Performance Solution‐Processed Bulk Heterojunction Solar Cells. *Advanced Materials* **2013**, *25*, 5898-5903.

(16) Liu, X.; Sun, Y.; Perez, L. A.; Wen, W.; Toney, M. F.; Heeger, A. J.; Bazan, G. C. Narrow-band-gap conjugated chromophores with extended molecular lengths. *Journal of the American Chemical Society* **2012**, *134*, 20609-20612.

(17) Liu, Y.; Chen, C.-C.; Hong, Z.; Gao, J.; Yang, Y. M.; Zhou, H.; Dou, L.; Li, G.; Yang, Y. Solution-processed small-molecule solar cells: breaking the 10% power conversion efficiency. *Scientific*

reports **2013**, *3*.

(18) Patra, D.; Chiang, C.-C.; Chen, W.-A.; Wei, K.-H.; Wu, M.-C.; Chu, C.-W. Solution-processed benzotrithiophene-based donor molecules for efficient bulk heterojunction solar cells. *Journal of Materials Chemistry A* **2013**, *1*, 7767-7774.

(19) Walker, B.; Tamayo, A. B.; Dang, X. D.; Zalar, P.; Seo, J. H.; Garcia, A.; Tantiwiwat, M.; Nguyen, T. Q. Nanoscale Phase Separation and High Photovoltaic Efficiency in Solution‐Processed, Small‐Molecule Bulk Heterojunction Solar Cells. *Advanced Functional Materials* **2009**, *19*, 3063-3069.

(20) Wang, H.; Liu, F.; Bu, L.; Gao, J.; Wang, C.; Wei, W.; Russell, T. P. The Role of Additive in Diketopyrrolopyrrole‐Based Small Molecular Bulk Heterojunction Solar Cells. *Advanced Materials* **2013**, *25*, 6519-6525.

(21) Winzenberg, K. N.; Kemppinen, P.; Scholes, F. H.; Collis, G. E.; Shu, Y.; Singh, T. B.; Bilic, A.; Forsyth, C. M.; Watkins, S. E. Indan-1, 3-dione electron-acceptor small molecules for solution-processable solar cells: a structure–property correlation. *Chemical Communications* **2013**, *49*, 6307-6309.

(22) Ye, D.; Li, X.; Yan, L.; Zhang, W.; Hu, Z.; Liang, Y.; Fang, J.; Wong, W.-Y.; Wang, X. Dithienosilole-bridged small molecules with different alkyl group substituents for organic solar cells exhibiting high open-circuit voltage. *Journal of Materials Chemistry A* **2013**, *1*, 7622-7629.

(23) Zhou, J.; Wan, X.; Liu, Y.; Zuo, Y.; Li, Z.; He, G.; Long, G.; Ni, W.; Li, C.; Su, X. Small molecules based on benzo [1, 2-b: 4, 5-b′] dithiophene unit for high-performance solution-processed organic solar cells. *Journal of the American Chemical Society* **2012**, *134*, 16345-16351.

(24) Zhou, J.; Zuo, Y.; Wan, X.; Long, G.; Zhang, Q.; Ni, W.; Liu, Y.; Li, Z.; He, G.; Li, C. Solution-processed and high-performance organic solar cells using small molecules with a benzodithiophene unit. *Journal of the American Chemical Society* **2013**, *135*, 8484-8487.

(25) Kan, B.; Li, M. M.; Zhang, Q.; Liu, F.; Wan, X. J.; Wang, Y. C.; Ni, W.; Long, G. K.; Yang, X.; Feng, H. R.; Zuo, Y.; Zhang, M. T.; Huang, F.; Cao, Y.; Russell, T. P.; Chen, Y. S. A Series of Simple Oligomer-like Small Molecules Based on Oligothiophenes for Solution-Processed Solar Cells with High Efficiency. *Journal of the American Chemical Society* **2015**, *137*, 3886-3893.

(26) Sumpter, B. G.; Meunier, V. Can computational approaches aid in untangling the inherent complexity of practical organic photovoltaic systems? *Journal of Polymer Science Part B: Polymer Physics* **2012**, *50*, 1071-1089.

(27) Liu, F.; Gu, Y.; Jung, J. W.; Jo, W. H.; Russell, T. P. On the morphology of polymer‐based photovoltaics. *Journal of Polymer Science Part B: Polymer Physics* **2012**, *50*, 1018-1044.

(28) Ruderer, M. A.; Müller-Buschbaum, P. Morphology of polymer-based bulk heterojunction films for organic photovoltaics. *Soft Matter* **2011**, *7*, 5482-5493.

(29) Zhou, J.; Zuo, Y.; Wan, X.; Long, G.; Zhang, Q.; Ni, W.; Liu, Y.; Li, Z.; He, G.; Li, C.; Kan, B.; Li, M.; Chen, Y. Solution-processed and high-performance organic solar cells using small molecules with a benzodithiophene unit. *Journal of the American Chemical Society* **2013**, *135*, 8484-8487.

(30) Liu, Y.; Chen, C. C.; Hong, Z.; Gao, J.; Yang, Y. M.; Zhou, H.; Dou, L.; Li, G.; Yang, Y. Solution-processed small-molecule solar cells: breaking the 10% power conversion efficiency. *Scientific reports* **2013**, *3*, 3356.

(31) Zhou, J.; Wan, X.; Liu, Y.; Zuo, Y.; Li, Z.; He, G.; Long, G.; Ni, W.; Li, C.; Su, X.; Chen, Y. Small molecules based on benzo[1,2-b:4,5-b']dithiophene unit for high-performance solution-processed organic solar cells. *Journal of the American Chemical Society* **2012**, *134*, 16345-16351.

(32) Lee, J. K.; Ma, W. L.; Brabec, C. J.; Yuen, J.; Moon, J. S.; Kim, J. Y.; Lee, K.; Bazan, G. C.; Heeger,

A. J. Processing additives for improved efficiency from bulk heterojunction solar cells. *Journal of the American Chemical Society* **2008**, *130*, 3619-3623.

(33) Park, J. K.; Walker, B.; Seo, J. H. Controlling polarity of organic bulk heterojunction field-effect transistors via solvent additives. *ACS applied materials & interfaces* **2013**, *5*, 4575-4580.

(34) Hoogerbrugge, P.; Koelman, J. Simulating microscopic hydrodynamic phenomena with dissipative particle dynamics. *EPL (Europhysics Letters)* **1992**, *19*, 155.

(35) Koelman, J.; Hoogerbrugge, P. Dynamic simulations of hard-sphere suspensions under steady shear. *EPL (Europhysics Letters)* **1993**, *21*, 363.

(36) Groot, R. D.; Madden, T. J. Dynamic simulation of diblock copolymer microphase separation. *The Journal of Chemical Physics* **1998**, *108*, 8713.

(37) Li, Y.; He, X.; Cao, X.; Shao, Y.; Li, Z.; Dong, F. Mesoscopic simulation study on the efficiency of surfactants adsorbed at the liquid/liquid interface. *Molecular Simulation* **2005**, *31*, 1027-1033.

(38) Wodo, O.; Tirthapura, S.; Chaudhary, S.; Ganapathysubramanian, B. A graph-based formulation for computational characterization of bulk heterojunction morphology. *Organic Electronics* **2012**, *13*, 1105-1113.

(39) Lei, B.; Yao, Y.; Kumar, A.; Yang, Y.; Ozolins, V. Quantifying the relation between the morphology and performance of polymer solar cells using Monte Carlo simulations. *Journal of Applied Physics* **2008**, *104*, 024504.

(40) Buxton, G. A.; Clarke, N. Predicting structure and property relations in polymeric photovoltaic devices. *Physical Review B* **2006**, *74*, 085207.

(41) Min Nam, Y.; Huh, J.; Ho Jo, W. Optimization of thickness and morphology of active layer for high performance of bulk-heterojunction organic solar cells. *Solar Energy Materials and Solar Cells* **2010**, *94*, 1118-1124.

(42) Watkins, P. K.; Walker, A. B.; Verschoor, G. L. B. Dynamical Monte Carlo Modelling of Organic Solar Cells: The Dependence of Internal Quantum Efficiency on Morphology. *Nano Letters* **2005**, *5*, 1814-1818.

(43) Lin, B. C.; Koo, B. T.; Clancy, P.; Hsu, C. P. Theoretical Investigation of Charge-Transfer Processes at Pentacene-C-60 Interface: The Importance of Triplet Charge Separation and Marcus Electron Transfer Theory. *Journal of Physical Chemistry C* **2014**, *118*, 23605-23613.

(44) Sun, H. COMPASS: An ab initio force-field optimized for condensed-phase applications - Overview with details on alkane and benzene compounds. *Journal of Physical Chemistry B* **1998**, *102*, 7338-7364.

(45) Rigby, D.; Sun, H.; Eichinger, B. E. Computer simulations of poly(ethylene oxide): force field, pvt diagram and cyclization behaviour. *polymer international* **1997**, *44*, 311-330.

(46) Xue, J.; Hou, T.; Li, Y. Optimal parameters for morphology of bulk heterojunction solar cells from simulations. *Applied Physics Letters* **2012**, *100*, 053307.

(47) Kozub, D. R.; Vakhshouri, K.; Orme, L. M.; Wang, C.; Hexemer, A.; Gomez, E. D. Polymer Crystallization of Partially Miscible Polythiophene/Fullerene Mixtures Controls Morphology. *Macromolecules* **2011**, *44*, 5722-5726.

(48) Machui, F.; Langner, S.; Zhu, X.; Abbott, S.; Brabec, C. J. Determination of the P3HT:PCBM solubility parameters via a binary solvent gradient method: Impact of solubility on the photovoltaic performance. *Solar Energy Materials and Solar Cells* **2012**, *100*, 138-146.

(49) Groot, R.; Rabone, K. Mesoscopic simulation of cell membrane damage, morphology change and rupture by nonionic surfactants. *Biophysical journal* **2001**, *81*, 725-736.

(50) Martys, N. S.; Mountain, R. D. Velocity Verlet algorithm for dissipative-particle-dynamics-based models of suspensions. *Physical Review E* **1999**, *59*, 3733.

(51) Flory; J., P.: *Principles of polymer chemistry*; Cornell University Press, 1953.

(52) Maiti, A.; McGrother, S. Bead–bead interaction parameters in dissipative particle dynamics: relation to bead-size, solubility parameter, and surface tension. *The Journal of Chemical Physics* **2004**, *120*, 1594.

(53) Zhao, Y.; You, L.-Y.; Lu, Z.-Y.; Sun, C.-C. Dissipative particle dynamics study on the multicompartment micelles self-assembled from the mixture of diblock copolymer poly (ethyl ethylene)-< i> block</i>-poly (ethylene oxide) and homopolymer poly (propylene oxide) in aqueous solution. *Polymer* **2009**, *50*, 5333-5340.

(54) Sun, H. COMPASS: An ab initio force-field optimized for condensed-phase applications overview with details on alkane and benzene compounds. *The Journal of Physical Chemistry B* **1998**, *102*, 7338-7364.

(55) Sun, H.; Ren, P.; Fried, J. The COMPASS force field: parameterization and validation for phosphazenes. *Computational and Theoretical Polymer Science* **1998**, *8*, 229-246.

(56) Yang, J.; Ren, Y.; Tian, A.-m.; Sun, H. COMPASS force field for 14 inorganic molecules, He, Ne, Ar, Kr, Xe, H2, O2, N2, NO, CO, CO2, NO2, CS2, and SO2, in liquid phases. *The Journal of Physical Chemistry B* **2000**, *104*, 4951-4957.

(57) Petrus, P.; Lisal, M.; Brennan, J. K. Self-assembly of symmetric diblock copolymers in planar slits with and without nanopatterns: Insight from dissipative particle dynamics simulations. *Langmuir : the ACS journal of surfaces and colloids* **2009**, *26*, 3695-3709.

(58) Li, Z.-W.; Lu, Z.-Y.; Sun, Z.-Y.; Li, Z.-S.; An, L.-J. Calculating the equation of state parameters and predicting the spinodal curve of isotactic polypropylene/poly (ethylene-co-octene) blend by molecular dynamics simulations combined with Sanchez-Lacombe lattice fluid theory. *The Journal of Physical Chemistry B* **2007**, *111*, 5934-5940.

(59) Sun, Y.; Welch, G. C.; Leong, W. L.; Takacs, C. J.; Bazan, G. C.; Heeger, A. J. Solution-processed small-molecule solar cells with 6.7% efficiency. *Nature materials* **2012**, *11*, 44-48.

(60) Ko Ko Kyaw, A.; Hwan Wang, D.; Tseng, H.-R.; Zhang, J.; Bazan, G. C.; Heeger, A. J. Electron and hole mobility in solution-processed small molecule-fullerene blend: Dependence on the fullerene content. *Applied Physics Letters* **2013**, *102*, 163308.

(61) Venturoli, M.; Smit, B.; Sperotto, M. M. Simulation Studies of Protein-Induced Bilayer Deformations, and Lipid-Induced Protein Tilting, on a Mesoscopic Model for Lipid Bilayers with Embedded Proteins. *Biophysical Journal* **2005**, *88*, 1778-1798.

(62) Li, X.; Pivkin, I. V.; Liang, H.; Karniadakis, G. E. Shape Transformations of Membrane Vesicles from Amphiphilic Triblock Copolymers: A Dissipative Particle Dynamics Simulation Study. *Macromolecules* **2009**, *42*, 3195-3200.

(63) Graham, K. R.; Mei, J.; Stalder, R.; Shim, J. W.; Cheun, H.; Steffy, F.; So, F.; Kippelen, B.; Reynolds, J. R. Polydimethylsiloxane as a macromolecular additive for enhanced performance of molecular bulk heterojunction organic solar cells. *ACS Applied Materials & Interfaces* **2011**, *3*, 1210-1215.

(64) Ma, W.; Yang, C.; Gong, X.; Lee, K.; Heeger, A. J. Thermally Stable, Efficient Polymer Solar Cells with Nanoscale Control of the Interpenetrating Network Morphology. *Advanced Functional Materials* **2005**, *15*, 1617-1622.

(65) Verploegen, E.; Mondal, R.; Bettinger, C. J.; Sok, S.; Toney, M. F.; Bao, Z. Effects of Thermal

Annealing Upon the Morphology of Polymer–Fullerene Blends. *Advanced Functional Materials* **2010**, *20*, 3519-3529.

(66) Graham, K. R.; Wieruszewski, P. M.; Stalder, R.; Hartel, M. J.; Mei, J.; So, F.; Reynolds, J. R. Improved Performance of Molecular Bulk-Heterojunction Photovoltaic Cells through Predictable Selection of Solvent Additives. *Advanced Functional Materials* **2012**, *22*, 4801-4813.